A Microfluidic Organotypic Device for Culture of Mammalian Intestines Ex Vivo

Journal:	*Analytical Methods*
Manuscript ID	AY-ART-09-2019-002038.R1
Article Type:	Paper
Date Submitted by the Author:	26-Nov-2019
Complete List of Authors:	Richardson, Alec; Colorado State University, Biomedical Engineering Schwerdtfeger, Luke; Colorado State University, Biomedical Sciences Eaton, Diana; Applied Medical McLean, Ian; Colorado State University, Biomedical Engineering Tobet, Stuart; Colorado State University, Biomedical Engineering Henry, Charles; Colorado State University, Chemistry;

1
2
3   1
4
5
6   2
7
8
9   3
10
11
12   4   **A Microfluidic Organotypic Device for Culture of Mammalian Intestines Ex Vivo**
13

14
15   5   Alec Richardson[1,3], Luke A. Schwerdtfeger[2], Diana Eaton[4], Ian Mclean[3], Charles S. Henry[1,3,*],
16
17   6   Stuart A. Tobet[2,3,*]
18
19   7   Department of Chemistry[1], Department of Biomedical Sciences[2], School of Biomedical
20
21   8   Engineering[3], Colorado State University, Fort Collins, Colorado, 80523
22
23
24   9   Applied Medical Resources Corporation[4], Rancho Santa Margarita, California, 92688
25
26
27   10   **Corresponding Authors:**
28
29   11   **Dr. Stuart A. Tobet**
30
31   12   Department of Biomedical Sciences, 1617 Campus Delivery
32
33   13   Fort Collins, CO 80523-1617
34
35   14   Phone: 970 491 1672
36
37   15   email: stuart.tobet@colostate.edu
38
39   16   **Dr. Charles S. Henry**
40
41
42   17   Department of Chemistry, 1872 Campus Delivery
43
44
45   18   Colorado State University
46
47
48   19   Fort Collins, CO 80523
49
50   20   Phone: 970 491 2852
51
52
53   21   Email:chuck.henry@colostate.edu
54
55
56
57

Abstract:

The physiological characteristics of the gastrointestinal (GI) tract are diverse and include rapid rates of epithelial turnover, complex nervous and immune systems, a thick mucus layer, and a large microbial population. Most GI models in vitro rely upon cell lines or organoids and consequently lack the diversity of cells and microorganisms present in vivo. In vivo studies retain function and cellular diversity but are more difficult to control. Microfluidic tissue-on-a-chip devices provide powerful alternatives for modeling physiological systems. Such devices show promise for use in GI research; however, most models use non-physiologic culture environments with higher than in vivo oxygen levels and insufficient gut microbiota. Our goal is to create a bridge between in vitro and in vivo using microfluidic devices by incorporating ex vivo tissue explants in physiologically relevant environments. Here, we report a microfluidic organotypic device (MOD) that enables media flow with differential oxygen concentrations across luminal and muscular surfaces of gut tissue ex vivo. Tissue was shown to be viable for 72 h and lowering oxygen concentration to a more physiologic level impacted bacterial populations.

Keywords: Microfluidic, intestine, explant, ex vivo, organotypic

Introduction

Intestinal tissue is composed of a complex network of epithelial, neural, immune, muscular, and vascular components.[1] Bacteria that inhabit the intestinal lumen are major contributors to maintaining intestinal homeostasis. An imbalance in microbial communities (dysbiosis) is associated with a variety of local tissue diseases such as inflammatory bowel (IBD) and celiac disease.[2,3] More globally, dysbiosis influences disorders ranging from

46 cardiovascular disease to brain function.[4,5] For in vitro and ex vivo intestinal models, cellular

47 diversity and recapitulation of the in vivo environment is paramount to better understanding the

48 relationship between dysbiosis and disease. For instance, bacterial cell products can activate

49 intestinal neurons, leading to the release of inflammatory cytokines associated with IBD.[6]

50 Traditional in vitro cell culture can recapitulate some aspects of intestinal physiology and is

51 useful for high throughput screening, but these models often rely upon cell monolayers to

52 represent the intestinal barrier. Cell monolayers lack the in vivo cellular diversity from both a

53 mammalian host and bacterial perspective and do not accurately represent the three-

54 dimensional architecture of the intestinal wall.[7,8] Three-dimensional intestinal organoids

55 overcome some of these limitations by integrating multiple epithelial cell subtypes and exhibiting

56 villus/crypt organization, but they are generally missing the neural, immune, and muscular

57 components of the gut wall.[8,9]

58   Improving upon static transwell models, 'gut-on-a-chip' microfluidic devices have been

59 developed that allow media to be continuously perfused across opposing sides of a cell-seeded

60 porous membrane representing the intestinal epithelial barrier.[10-13] The incorporation of

61 microfluidics in these devices improves cellular viability and longevity, constantly removes toxic

62 cellular waste, and allows for controlled nutrient delivery.[14] Recently, microbes have been

63 incorporated into some *in vitro* microfluidic intestinal models by generating an oxygen gradient

64 between microfluidic channels.[15-19]

65   Organotypic intestinal culture models are an attractive middle ground between *in vitro*

66 and *in vivo* systems because they include the three-dimensional architecture of the gut wall

67 while still providing easily controllable experimental parameters.[20] Ex vivo models of various

68 tissues have been successfully used in microfluidic devices previously.[21-25] *Ex vivo* models,

69 however, are generally low-throughput compared to cell-monolayer cultures and many have

70 limited long-term tissue viability.[8,26] The Ussing chamber is a well-established *ex vivo* model for

71   studying trans-epithelial drug, nutrient, and ion transport. While the Ussing chamber is valuable

72   for pharmacokinetic/pharmacodynamic studies, viable epithelial tissue can only be maintained

73   for several hours,[27,28] making these models inappropriate for long-term host tissue-microbiome

74   interaction studies.[29] In this report, we describe the design and testing of a microfluidic

75   organotypic device (MOD) for use with mammalian intestinal explants *ex vivo*. The MOD houses

76   full-thickness mouse intestinal tissue, including muscular, neural, immune, and epithelial

77   components. The MOD system was used to maintain mouse intestinal explants for 72 h, with

78   differential bacterial growth as a function of oxygen concentration.

79

80   **Methods**

81   Device prototypes were designed in SolidWorks (Dassault Systemes, Waltham, MA) and

82   3D printed with a Form 2 SLA printer (Formlabs, Somerville, MA). Once a final device design

83   was established, the MOD was manufactured via injection molding (Applied Medical, Rancho

84   Santa Margarita, CA) using cyclic olefin copolymer (COC; TOPAS Grade 8007) as material. All

85   devices used during tissue testing were injection molded. Injection molding was chosen over

86   other microfluidic device manufacturing methods because of its reproducibility and potential for

87   large-scale manufacturing.[30] COC was chosen because of its biocompatibility, high chemical

88   resistance, low oxygen permeability, and excellent optical properties.[31-33]

89   The MOD (Figure 1A) consists of three COC layers separated by polyurethane gaskets

90   (PORON® AquaPro™, Rogers Corporation, Chandler, AZ); the gaskets define independent

91   fluidic channels (10 mm wide, 1.1 mm deep, ~ 50 mm long, ~ 450 µL). Intestinal tissue is

92   housed in the middle layer such that the mucosa and serosa face independent channels. The

93   edge of the tissue is supported by a thin lip molded into the middle layer, eliminating the need

94   for a porous membrane. The top layer was designed with integrated snap-fit fasteners for rapid,

95   reversible assembly (Video S1), which is crucial to minimizing the time tissue explants are

96   without media. Unlike other fasteners, snap-fit fasteners can be injection molded and enable

97   consistent assembly regardless of the user. Both the top and bottom layers contain threaded

98   inlet and outlet ports that connect to 10-32 PEEK finger-tight fittings (IDEX Health & Science,

99   LLC, Oak Harbor, WA). Rubber O-rings were installed at the base of each port to ensure airtight

100   leakproof connections (IDEX Health & Science, LLC, Oak Harbor, WA). Glass coverslips (VWR,

101   Radnor, PA) were fixed on the top and bottom layers using cyanoacrylate glue (Krazy Glue,

102   Elmers Products, High Point, NC) directly above the tissue to enable on-chip imaging and tissue

103   visualization (VWR, Radnor, PA). Quick setting epoxy was applied around the edges of the

104   coverslips to further prevent leakage and the top and bottom layers were placed in a 65° C oven

105   for 15 min.

106   As a first step in instrumenting the device, oxygen sensor spots (OptiEnz, Fort Collins,

107   CO) were adhered to the inner surface of the top layer downstream of the tissue chamber. The

108   sensor's response was measured at two dissolved oxygen concentrations (DOC) using an

109   external fiber optic probe (OptiEnz, Fort Collins, CO) to allow for the estimation of real-time

110   DOC using the Stern-Volmer relationship:

$$\frac{\tau_0}{\tau} = 1 + K_{SV}[O_2] \quad , \tag{1}$$

112   where τ_0 is the luminescent decay time in the absence of oxygen, τ is the luminescent decay

113   time in the presence of oxygen, K_{SV} is the Stern-Volmer constant, and $[O_2]$ is the oxygen

114   concentration. Fluorescence of an oxygen-sensitive compound on the sensor spot is quenched

115   in the presence of oxygen, leading to a reduction in luminescent decay time.[34]

116   After assembly, each device was tested for failure modes, sterilized, and placed in a sterile

117   environment until use. All fittings, ferrules, and tubing were submerged in diluted (1:10) bleach

118   for 10 min, rinsed thoroughly with DI water, placed in a soapy water bath and vigorously

119   scrubbed. After a second DI water rinse, the components and devices were submerged in a

120   70% ethanol solution containing 0.1% benzalkonium chloride for 30 min and rinsed with sterile

121   water. Lastly, all other components including the gaskets and collection tubes were autoclaved

122   at 120°C for 25 min. The devices could not be autoclaved due to COC's glass transition

123   temperature of 78°C. Culture media was composed of CTS Neurobasal-A Medium (Thermo

124   Fisher Scientific, Waltham, MA), 5% (v/v) 1M HEPES Buffer (Sigma Aldrich, St. Louis, MO), 2%

125   (v/v) B-27 Supplement (Thermo Fisher Scientific, Waltham, WA) and supplemented with 10 µM

126   Nicardipine (Sigma Aldrich, St. Louis, MO), an L-type calcium ion channel blocker, that has

127   previously been shown to block intestinal contractions *ex vivo,* a necessity when culturing

128   intestinal tissue slices beyond 48 h.[35] CTS Neurobasal-A Medium was chosen as its

129   predecessor, neurobasal media, has proven reliable in maintaining healthy explant slices from

130   both mouse[35] and human[36] intestines, among numerous other organs[37, 38, 39]. For each device,

131   two syringes were filled with media (one containing 99.3 µM fluorescein), connected to NE-300

132   syringe pumps (New Era Pump Systems Inc., Farmingdale, NY) and equilibrated in a 37°C

133   incubator prior to experiments to remove any air bubbles formed by the expansion of dissolved

134   gasses in the media. Mouse tissue was prepared as previously described[35] from mice approved

135   under the Colorado State University IACUC protocol 17-720(A). Briefly, adult mice were

136   sacrificed and the entirety of the large intestine was removed and placed in 4° C 1X Krebs

137   buffer (in mM: 126 NaCl, 2.5 KCl, 2.5 CaCl$_2$, 1.2 NaH$_2$PO$_4$, 1.2 MgCl$_2$). The cecum was

138   removed and the colon was cut longitudinally along the mesenteric border to open the lumen

139   and form a flat sheet of tissue. Only ascending, transverse, and descending colon were used

140   for device experiments. Tissue was free-hand dissected to form slices with a diameter of ~5 mm

141   and placed in the center of the middle device layer. Cyanoacrylate glue was applied around the

142   perimeter of the tissue to fill gaps between the tissue and plastic. While cyanoacrylate glue has

143   been reported to be cytotoxic,[40] we only observed higher than expected levels of cell death

144   where the glue directly contacted the tissue. After securing the tissue in the middle device

145   layer, the device was quickly assembled by stacking successive layers separated by the

146   gaskets and snapping them together. The devices were placed in a 37° C incubator, connected

147   to syringes, and purged with media at a flow rate of 2.5 mL/hr. Media containing fluorescein was

148   perfused through the luminal channel while media without fluorescein was perfused through the

149   serosal channel. Once effluent media reached the collection tubes, the flow rate was reduced to

150   250 µL/hr for the remainder of the experiments to provide low shear stress across the tissue.

151   Collection tubes were changed every 10 h and immediately stored at -80°C. Colon explants

152   used for mucus experiments were cultured for 48 h before the addition of an azido-modified

153   galactosamine, Tetraacetylated N-Azidoacetylgalactosamine (GalNAz; 12.5 µM; Fisher

154   Scientific, Pittsburgh, PA). At the conclusion of experiments, tissue explants were removed from

155   the devices and placed in media containing either Ethidium Homodimer III (EtHD; Biotium,

156   Hayward, CA) at a concentration of 2.5 µM to evaluate cell death, or a fluorophore-tagged

157   alkyne, Dibenzocyclooctyne-Cy3 (DBCO-Cy3; 2 µM; Sigma-Aldrich, St. Louis, MO). After 30 min

158   of incubation with EtHD, or 15 min of incubation with DBCO-Cy3, tissue explants were washed

159   three times with culture media and fixed in 4% formaldehyde for a minimum of 8 h. Fixed tissue

160   was washed with, and stored in, cold 0.05 M PBS until further analysis. A total of 27 devices

161   were used for experiments, 4 of which were discarded due to breakage of the cyanoacrylate

162   barrier separating the fluidic channels.

163   Fixed explants were sectioned at 50 µm thick on a vibrating microtome (VT1000s, Leica

164   Microsystems, Wetzlar, Germany) before mounting on glass microscope slides. Imaging was

165   performed on a Nikon TE2000-U inverted microscope (20x Plan-Apo objective) with a UniBlitz

166   shutter system (Vincent Associates, Rochester, NY) and an Orca-flash 4.0 LT camera

167   (Hamamatsu, Hamamatsu City, Shizuoka Prefecture, Japan).

168   Fluorescein quantities contained in culture media effluents were analyzed using an

169   Epoch Gen5 Microplate Spectrophotometer (BioTek, Winooski, VT) with a wavelength of 488

170   nm. Absorbance was quantified in effluent media from both channels in 10 h increments, with

171   hour 0 representing initial placement of explants into devices. Background signal from phenol

172   red, a component of CTS Neurobasal Medium, was removed.

173

174

175   **Results and Discussion:**

176   Mouse colon explants were cultured in the MOD for up to 72 h *ex vivo* in both low and

177   ambient mucosal DOC maintaining healthy, intact tissue (Supplemental Figure 1A-C). Tissue

178   health was marked by maintenance of patterned rows of colonic crypts, with interspersed lamina

179   propria and stereotypic arrangement of intestinal submucosal and muscular layers (Figure 2A,

180   B, C). Minimal cell death was shown across 0h – 72h *ex vivo* (Figure 2D, E, F), indicated by

181   labelling with EtHD. As expected, some EtHD was observed at the apical most epithelium, but

182   not at the base of colonic crypts. Stem/progenitor cells at the base of colonic crypts proliferate

183   and progeny migrate along the length of the crypt, towards the luminal aspect, before

184   undergoing apoptosis and sloughing off into the intestinal lumen.[41] This cycle is continuously

185   repeated to regenerate a new epithelium every 2-3 days in the mouse.[42] Minimal cell death

186   observed throughout our explants during *ex vivo* culture, coupled with the EtHD signal at the

187   apical most aspect of the crypt, points towards healthy tissue undergoing normal epithelial

188   turnover. While others have maintained mammalian intestines in microfluidic devices for up to

189   72 h,[43] evidence of tissue health was minimal. Another concern in many systems[15, 43-45] is that

190   serum-containing media with supplemented antibiotics was used to culture the tissue. A key

191   advantage of the MOD is that we have maintained tissue in serum-free media, without

192   antibiotics, which enables controlled substance delivery to the tissue as well as studying the role

193   of bacteria on tissue health and physiology.

8

194   In addition to maintaining viable tissue for 72 h, media was separated in independent

195   microfluidic channels facing the mucosal and serosal sides of the tissue. Mean (+/- standard

196   deviation) absorbance across all time points for luminal effluents was 0.11 +/- 0.03 and 0.00 +/-

197   0.02 for serosal effluents, indicating that media did not cross channels throughout the duration

198   of the experiments (Figure 3). One potential concern is that fluorescein leakage could be diluted

199   by the fluid flow, under the spectrophotometer's detection limit. Since fluorescein and

200   fluorescein-isothiocyanate are commonly used to assess barrier permeability in vivo[46] and in

201   vitro,[47] any leakage below the detection limit is not biologically significant as an indication of

202   barrier disruption. If media had crossed through the tissue, absorbance values would have

203   increased substantially in the serosal effluent due to transfer or leakage of fluorescein across

204   the tissue. Another potential concern is the reliability of the cyanoacrylate seal around the

205   tissue. In ~15% of the devices tested, tissue lost adhesion to the cyanoacrylate glue and media

206   was allowed to freely transfer between channels. Future iterations of the MOD will be designed

207   to reduce device failure rates and increase experimental repeatability. The verification of media

208   separation is a critical indicator that the gut wall tissue retained one of its most essential

209   features *ex vivo*, that of a physical barrier with tight junctions between cells. This helps ensure

210   that pathogens, pharmaceuticals, and other compounds of interest for study *ex vivo* can only

211   access tissue physiology by going through normal cellular processes (e.g., active transport,

212   diffusion, cellular transfer). By comparison, in most organ-on-a-chip devices, a barrier is formed

213   by a confluent cell monolayer without the underlying cellular diversity needed to understand

214   intestinal physiology.

215   The MOD enabled recapitulation of the *in vivo* oxygen gradient across the epithelial

216   layer. DOC in the luminal channel were maintained at 3.0 +/- 0.38 mmHg for 48 h using 0.5 M

217   sodium sulfite. *In vivo* intraluminal oxygen concentrations at the mucosal interface are nearly

218   anoxic.[48] Perfusion of low oxygen-containing media within the luminal microfluidic channel

219 increased bacterial presence on the tissue's mucosal surface compared to tissue perfused with

220 media at ambient oxygen levels (~ 100 mmHg), as marked by fluorescent gram stain[35] (Figure

221 4A-F). Increases were most notable for gram-negative bacteria. Increased bacterial presence in

222 a low oxygen environment was expected since many bacteria in the colon are anaerobic.[49]

223 Therefore, recapitulation of the *in vivo* oxygen gradient is vital to studying host tissue

224 interactions with a more diverse, physiologically relevant bacterial community. It is also

225 important to note that these experiments are proof-of-principle. Quantifying specific bacteria and

226 overall bacteria concentrations will be the focus of future reports.

227 Microfluidics provide a mechanism of tissue perfusion ex vivo that should allow for

228 healthier tissue over longer periods.[14] Previous *ex vivo* systems such as intestinal organotypic

229 slices maintained tissue for 6 days, but without a true luminal barrier.[35] Other methods such as

230 Ussing chambers maintain full thickness tissues with an intact barrier, but with limited viability

231 over a few hours.[27] Using dual flow microfluidics, the MOD allows for the culture of full

232 thickness explants with an intact barrier over an extended length of culture (3 days).

233

Conclusion:

235 In conclusion, a novel *ex vivo* microfluidic organotypic device was designed and tested.

236 This system maintains viable polarized murine intestinal explants for 72 h *ex vivo* and enables a

237 physiological oxygen gradient to be established between independent microfluidic channels

238 rendering luminal and vascular compartments. The MOD bridges a substantial gap in current

239 approaches to modeling barrier tissue as it overcomes several limitations associated with both

240 *in vitro* and *in vivo* models. Due to the culture of full thickness explants, the MOD more closely

241 recapitulates the *in vivo* physiology of the gut wall, as tissue explants include the complex

1
2
3
4
5
6
7
8
9
10
11
12
13
14
15
16
17
18
19
20
21
22
23
24
25
26
27
28
29
30
31
32
33
34
35
36
37
38
39
40
41
42
43
44
45
46
47
48
49
50
51
52
53
54
55
56
57
58
59
60

242   cellular diversity and native tissue structural relationships of the gut wall. The MOD system

243   offers a novel approach to culturing intestinal tissues with intact luminal barriers.

244   Future extensions to the MOD will include developing and integrating optical and/or

245   electrochemical sensors for analytes relevant to the intestinal environment (i.e. glucose,

246   lactate). Electrodes can be added to assess transepithelial electrical resistance, which has been

247   a useful measure of barrier integrity in other systems.[15,50,51] Ultimately, the MOD will be

248   implemented in long-term microbiome studies to elucidate the relationship among microbial,

249   epithelial, neuro and immune components of the gut wall in health and disease.

250

251

252

253

266

267

268   **Figure Legends:**

269   Figure 1.

270   Schematic illustration of the MOD design and maintenance of tissue explants *ex vivo*. (A) an

271   exploded model of the MOD system showing luminal (red) and serosal (blue) flow paths. (B)

272   image of mouse colon explant inside the MOD. (C) image of colon explant tissue at 0h *ex vivo*

273   through the viewing window. (D) image of different colon explant tissue at 72 h *ex vivo* through

274   viewing window. Scale bars in C and D are 2 mm.

275

276   Figure 2.

277   Tissue health was maintained for 72 h *ex vivo* in the MOD in both ambient and low oxygen

278   conditions. Brightfield images in A-C demonstrate patterned rows of colonic crypts, and

279   stereotypic anatomical arrangement of gut wall musculature and submucosa at 0h (A), 72 h in

280   ambient oxygen (B) and 72 h in low oxygen (C). Fluorescent images in D-F demonstrate EtHD

281   labelling in colonic explants, with stereotypic signal observed at apical most aspect of colonic

282   crypts (arrows) at 0h (D), 72 h in ambient oxygen (E) and 72h in low oxygen (F). 'L' denotes

283   intestinal lumen, 'm' indicates mucosa, 'sm' submucosa, and 'me' muscularis externa. Scale

284   bars in A and B are 100 µm, scale bar in C is 50 µm, and scale bars in D-F are 25 µm.

285

286   Figure 3.

287   Media was separated across channels as marked by fluorescein absorbance in effluent media.

288   Mean absorbance (A.U.) at 488 nm wavelength demonstrates significantly more fluorescein

289   presence in mucosal (circular points) effluents compared to serosal (square points) (P < 0.001).

290   No significant differences were observed across time in either the mucosal (P > 0.20) or serosal

291   (P > 0.45) effluents. All statistical analyses were performed using a one-way ANOVA with α =

292   .05. Representative images show visible green color from fluorescein in mucosal (m) effluent

293   compared to serosal (s) effluent.

294

295   Figure 4.

296   Microbiota were maintained in the MOD, and more bacteria were visible in an explant cultured

297   in lower oxygen conditions. Baseline bacterial levels are shown at 0h ex vivo via hexidium

298   iodide (7.05 µM) fluorescence in red (A), signifying Gram-positive bacteria, and SYTO9 (5.01

299   µM) fluorescence in green (A'), signifying Gram-negative bacteria. Gram stain fluorescence

300   was noticeably higher in tissue cultured in lowered oxygen conditions (B-B'; 3 mmHg) when

301   compared to tissue cultured in ambient oxygen (C-C'; 100 mmHg) containing media. Arrows in

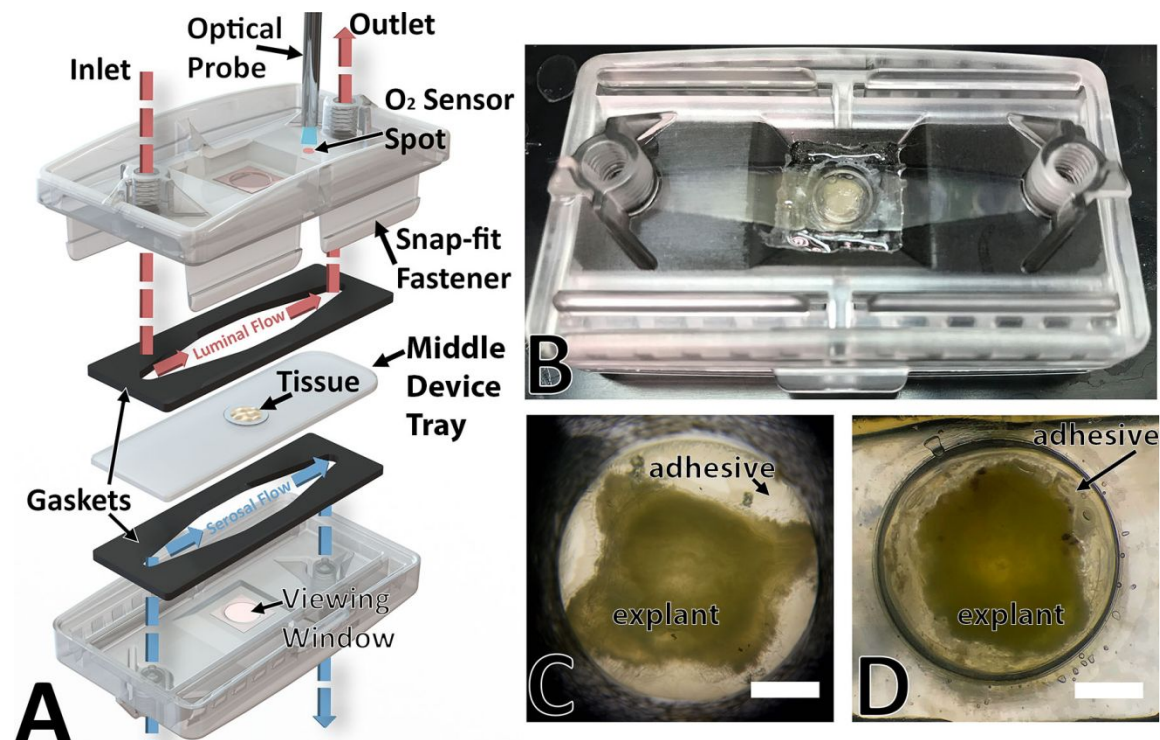302   A', B' and C' denote a single colonic crypt. Scale bars in all panels are 100 µm.

303

304   Supplemental Figure 1.

305   Tissue structure was maintained intact and patterned in stereotypic rows of colonic crypts at 72h

306   ex vivo. The images show representative sections cut at 50 µm of perfused mouse colon (A),

307   explants cultured in low DOC (B), and those cultured in ambient DOC (C). Sections were

308   stained with aldehyde fuchsin to elucidate general tissue structure and visualize colonic goblet

309   cells (e.g., arrows). 'L' represents intestinal lumen and 'c' a colonic crypt. Scale bars in A-C are

310   25 µm.

311

14

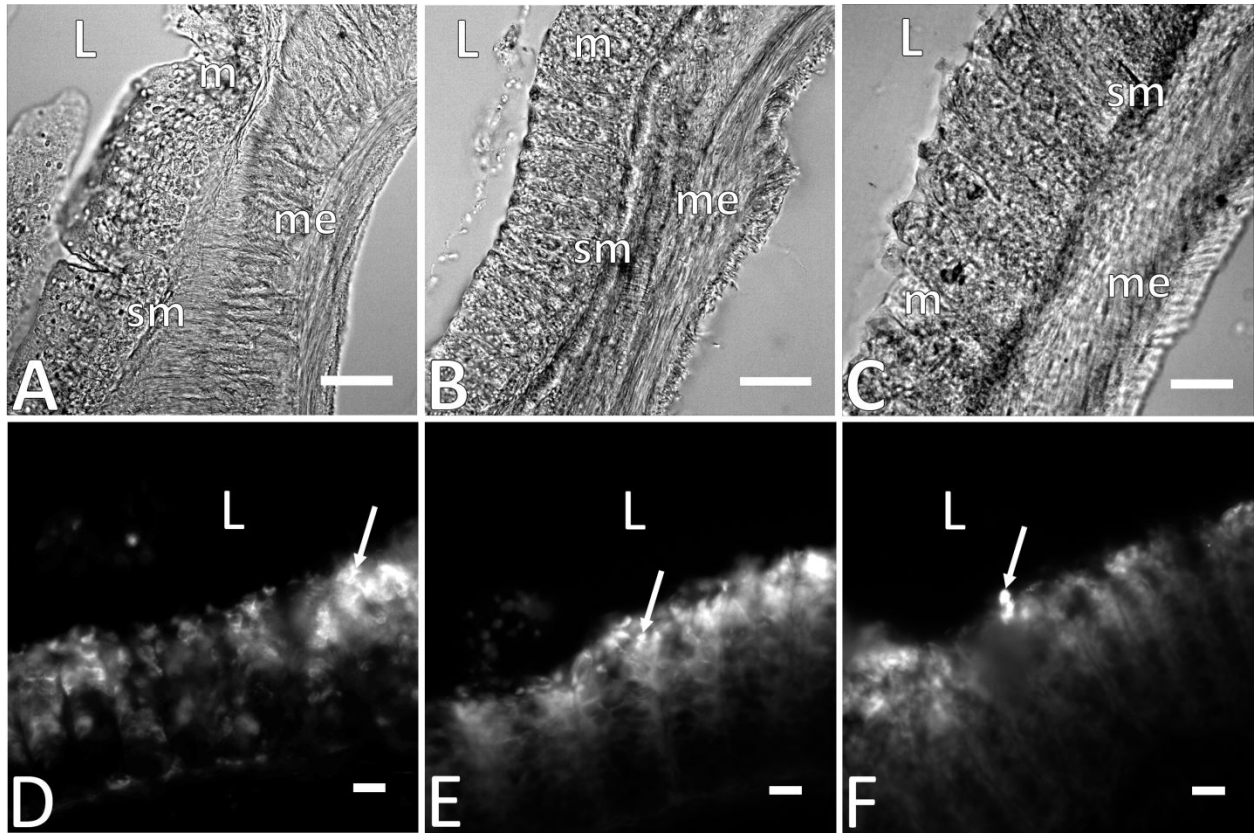312 **Figures:**

313 Figure 1.

314

315

316

317

318

319   Figure 2.

1
2
3   330   **Figure 3.**
4
5
6
7
8
9
10
11
12
13
14
15
16
17
18
19
20
21
22
23
24
25
26
27
28   331

29
30
31
32
33
34
35
36
37
38
39
40
41
42
43
44
45
46
47
48
49
50
51
52
53
54
55
56
57
58
59
60
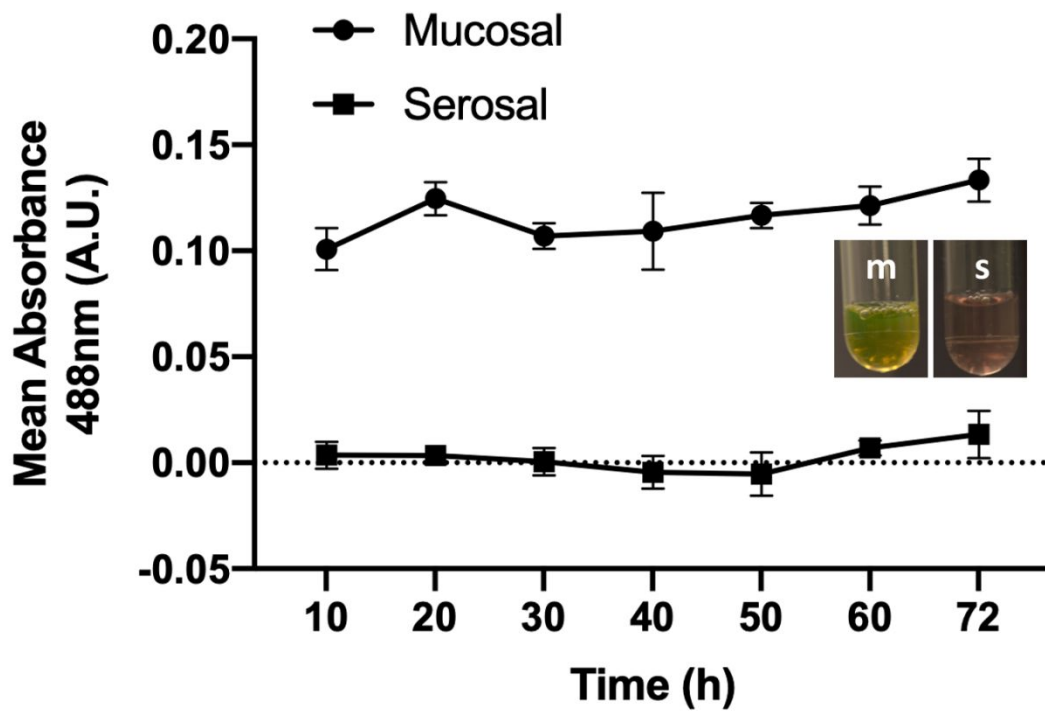
332 **Figure 4.**
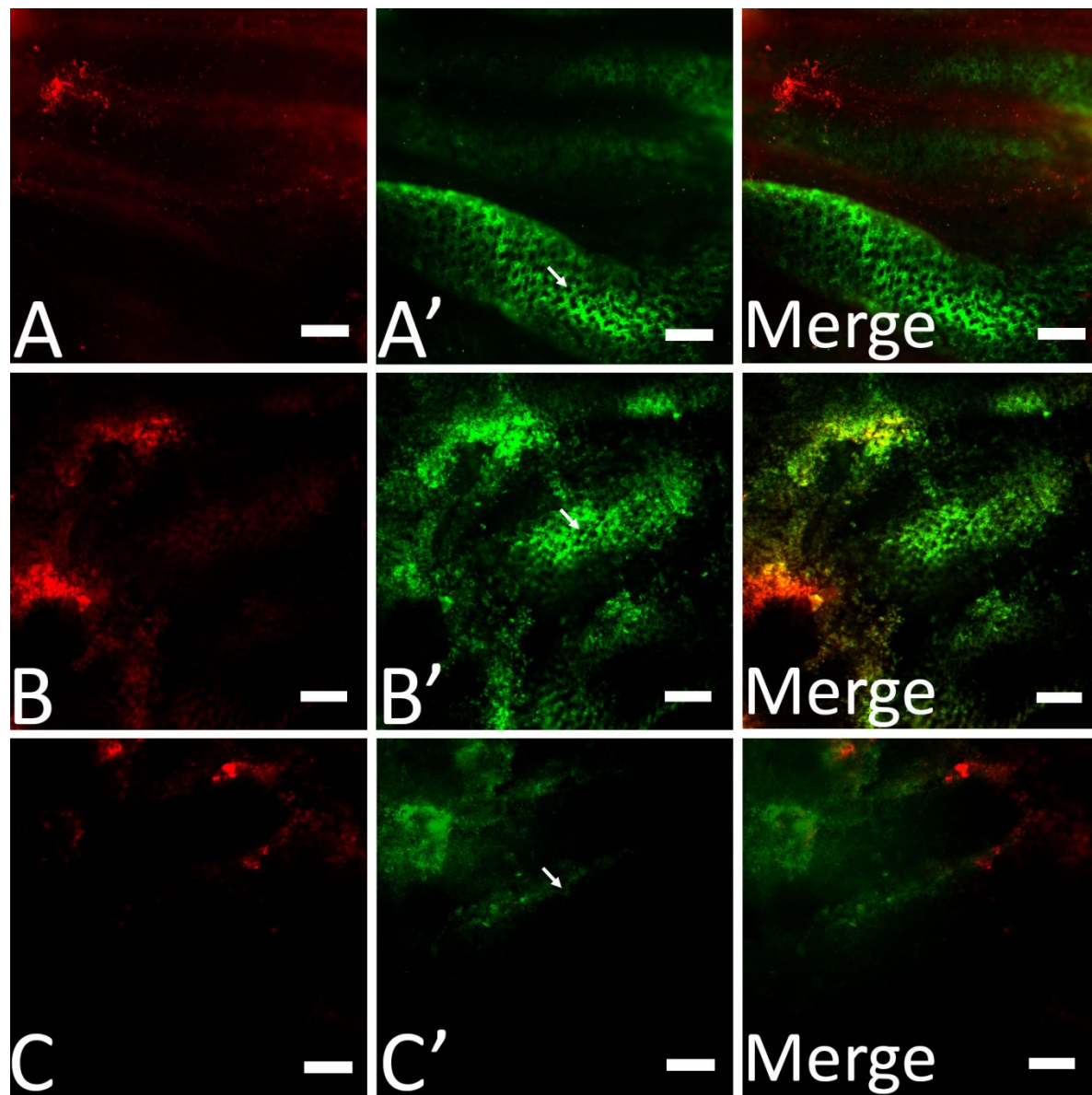
References:

1. J. M. Wells, O. Rossi, M. Meijerink and P. van Baarlen, *Proc. Natl. Acad. Sci.*, 2010, **108**, 4607–4614.

2. S. Ghaisas, J. Maher and A. Kanthasamy, *Pharmacol. Ther.*, 2016, **158**, 52–62.

3. S. Carding, K. Verbeke, D. Vipond, B. Corfe and L. Owen, *Microb. Ecol. Heal. Dis.*, 2015, **26**, 26191.

4. A. B. Shreiner, J. Y. Kao and V. B. Young, *Curr Opin Gastroenterol*, 2015, **31**, 69–75.

5. H. Jiang, Z. Ling, Y. Zhang, H. Mao, Z. Ma, Y. Yin, W. Wang, W. Tang, Z. Tan, J. Shi, L. Li and B. Ruan, *Brain. Behav. Immun.*, 2015, **48**, 186–194.

6. C. Bernardazzi, B. Pêgo and H. S. P. De Souza, *Mediators Inflamm.*, 2016, DOI:10.1155/2016/1363818.

7. T. Lea, in *The Impact of Food Bioactives on Health*, 2015, pp. 103–111.

8. A. Bein, W. Shin, S. Jalili-firoozinezhad, M. H. Park, A. Sontheimer-phelps, A. Tovaglieri, A. Chalkiadaki, H. J. Kim and D. E. Ingber, *Cell. Mol. Gastroenterol. Hepatol.*, 2018, **5**, 659–668.

9. L. A. Schwerdtfeger and S. A. Tobet, *J. Neuroendocrinol.*, 2018, e12650.

10. H. J. Kim and D. E. Ingber, *Integr. Biol.*, 2013, **5**, 1130.

11. K. Y. Shim, D. Lee, J. Han, N. T. Nguyen, S. Park and J. H. Sung, *Biomed. Microdevices*, 2017, **19**, 37.

12. W. Shin and H. J. Kim, *Proc. Natl. Acad. Sci.*, 2018, **115**, E10539–E10547.

13. M. B. Esch, J. H. Sung, J. Yang, C. Yu, J. Yu, J. C. March and M. L. Shuler, *Biomed. Microdevices*, 2012, **14**, 895–906.

14. I. C. Mclean, L. A. Schwerdtfeger, S. A. Tobet and C. S. Henry, *Lab Chip*, 2018, **18**, 1399–1410.

15. P. Shah, J. V. Fritz, E. Glaab, M. S. Desai, K. Greenhalgh, A. Frachet, M. Niegowska, M. Estes, C. Jäger, C. Seguin-Devaux, F. Zenhausern and P. Wilmes, *Nat. Commun.,* 2016, 7:11535, DOI:10.1038/ncomms11535.

16. M. Marzorati, B. Vanhoecke, T. De Ryck, M. S. Sadabad, I. Pinheiro, S. Possemiers, P. Van Den Abbeele, L. Derycke, M. Bracke, J. Pieters, T. Hennebel, H. J. Harmsen, W. Verstraete and T. Van De Wiele, *BMC Microbiology*, 2014, **14**, 133.

17. H. J. Kim, H. Li, J. J. Collins and D. E. Ingber, *Proc. Natl. Acad. Sci.*, 2015, **113**, E7–E15.

18. W. Shin, A. Wu, M. W. Massidda, C. Foster, N. Thomas, D.-W. Lee, H. Koh, Y. Ju, J. Kim and H. J. Kim, *Front. Bioeng. Biotechnol.*, 2019, **7**, 1–13.

19. S. Jalili-Firoozinezhad, F. S. Gazzaniga, E. L. Calamari, D. M. Camacho, C. W. Fadel, A. Bein, B. Swenor, B. Nestor, M. J. Cronce, A. Tovaglieri, O. Levy, K. E. Gregory, D. T. Breault, J. M. S. Cabral, D. L. Kasper, R. Novak and D. E. Ingber, *Nat. Biomed. Eng.*, , DOI:10.1038/s41551-019-0397-0.

20. R. Nunes, C. Silva and L. Chaves, in *Concepts and Models for Drug Permeability Studies: Cell and Tissue Based in Vitro Culture Models*, 2016, pp. 203-236.

21. S. Xiao, J. R. Coppeta, H. B. Rogers, B. C. Isenberg, J. Zhu, S. A. Olalekan, K. E. McKinnon, D. Dokic, A. S. Rashedi, D. J. Haisenleder, S. S. Malpani, C. A. Arnold-Murray, K. Chen, M. Jiang, L.

Bai, C. T. Nguyen, J. Zhang, M. M. Laronda, T. J. Hope, K. P. Maniar, M. E. Pavone, M. J. Avram, E. C. Sefton, S. Getsios, J. E. Burdette, J. J. Kim, J. T. Borenstein and T. K. Woodruff, Nat. Commun., 2017, 8, 14584.

22. A. E. Ross, M. C. Belanger, J. F. Woodroof and R. R. Pompano, Analyst, 2017, 142, 649.

23. K. H. Dodson, F. D. Echevarria, D. Li, R. M. Sappington and J. F. Edd, Biomed. Microdevices, 2015, 17, 114.

24. B. Atac, I. Wagner, R. Horland, R. Lauster, U. Marx, A. G. Tonevitsky, R. P. Azar and G. Lindner, Lab Chip, 2013, 13, 3555–3561.

25. S. Yasotharan, S. Pinto, J. G. Sled, S.-S. Bolz and A. Günther, Lab Chip, 2015, 15, 2660–2669.

26. S. C. Pearce, H. G. Coia, J. P. Karl, I. G. Pantoja-Feliciano, N. C. Zachos and K. Racicot, *Front Physiol.*, 2018, **9**, 1584

27. L. L. Clarke, *Am J Physiol Gastrointest Liver Physiol.*, 2009, **296**, 1151–1166.

28. B. Kisser, E. Mangelsen, C. Wingolf, L. I. Partecke, C. Heidecke, C. Tannergren, S. Oswald and M. Keiser, *Curr Protoc Pharmacol.,* 2017, **77**, 1–19.

29. S. May, S. Evans and L. Parry, *Emerg. Top. Life Sci.*, 2017, **1**, 385–400.

30. G. S. Fiorini and D. T. Chiu, *Biotechniques*, 2005, **38**, 429–446.

31. M. Berenguel-alonso, M. Sabés-alsina, R. Morató, O. Ymbern, L. Rodríguez-vázquez, O. Talló-parra, J. Alonso-chamarro, M. Puyol and M. López-béjar, *SLAS Technol.*, 2017, **22**, 507–517.

32. P. M. Van Midwoud, A. Janse, M. T. Merema, G. M. M. Groothuis and E. Verpoorte, *Anal. Chem.*, 2012, **84**, 3938–3944.

33. C. J. Ochs, J. Kasuya, A. Pavesi and R. D. Kamm, *Lab Chip*, 2014, **14**, 459–462.

34. X. D. Wang and O. S. Wolfbeis, *Chem. Soc. Rev.*, 2014, **43**, 3666–3761.

35. L. A. Schwerdtfeger, E. P. Ryan and S. A. Tobet, *Am J Physiol Gastrointest Liver Physiol*, 2016, **310**, 240–248.

36. L. A. Schwerdtfeger, N. J. Nealon, E. P. Ryan and S. A. Tobet, PloS one, 2019, 14, e0217170.

37. E. P. Bless, H. J. Walker, K. W. Yu, J. G. Knoll, S. M. Moenter, G. A. Schwarting and S. A. Tobet, Endocrinology, 2005, 146, 463-468.

38. A. M. Navratil, J. G. Knoll, J. D. Whitesell, S. A. Tobet and C. M. Clay, Endocrinology, 2007, 148, 1736-1744.

39. W. Tedjo, J. E. Nejad, R. Feeny, L. Yang, C. S. Henry, S. Tobet and T. Chen, Biosens Bioelectron, 2018, 114, 78-88.

40. P. A. Leggat, U. Kedjarune and D. R. Smith, *Ind. Health*, 2004, **42**, 207–211.

41. J. M. Allaire, S. M. Crowley, H. T. Law, S. Y. Chang, H. J. Ko and B. A. Vallance, *Trends Immunol.*, 2018, **39**, 677–696.

42. H. Chong and M. Bjerknes, *Anat Rec.*, 1983, **207**, 423-434

43. A. Dawson, C. Dyer, J. Macfie, J. Davies, L. Karsai, J. Greenman and M. Jacobsen, *Biomicrofluidics*, 2016, **10**, DOI:10.1063/1.4964813.

44. S. Oh, H. Ryu, D. Tahk, J. Ko, Y. Chung, H. K. Lee, T. R. Lee and N. L. Jeon, *Lab Chip*, 2017, **17**, 3405–3414.

45. M. Astolfi, F. Saad, F. Monet, E. Carmona, B. Péant, M. A. Lateef, J. Kendall-Dupont, A.-M. Mes-Masson, N. Rousset, T. Gervais and D. Provencher, *Lab Chip*, 2016, **16**, 312–325.

419   46. E. A. Vicuna, V.A. Kuttappan, R. Galarza-Seeber, J.D. Latorre, O.B. Faulkner, B.M. Hargis, G.
420   Tellez, L. R. Bielke, Poultry Science, 2015, 94, 2075-2080.

421   47. L. Zhang, J. Song, T. Bai, W. Qian, X. Hou, Scientific Reports, 2017, 7, 4950.

422   48. L. Albenburg, T. V. Esipova, C. Judge, K. Bittinger, J. Chen, A. Laughlin, S. Grunberg, R. N.
423   Baldassano, J. D. Lewis, H. Li, S. R. Thom, F. D. Bushman, S. A. Vinogradov and G. Wu,
424   *Gastroenterology*, 2014, **147**, 1055–1063.

425   49. W. Shin, A. Wu, M. W. Massidda, C. Foster, N. Thomas, D.-W. Lee, H. Koh, Y. Ju, J. Kim
426   and H. J. Kim, *Front. Bioeng. Biotechnol.*, 2019, **7**, 1–13.

427   50. O. Y. F. Henry, R. Villenave, M. J. Cronce, W. D. Leineweber, M. A. Benz and D. E. Ingber, *Lab
428   Chip*, 2017, **17**, 2264–2271.

429   51. J. J. Srinivasan, B.; Kolli, A.R.; Esch, M.B.; Abaci, H.E.; Shuler, L.; Hickman, B. Srinivasan, A. R.
430   Kolli, M. B. Esch, H. E. Abaci, M. L. Shuler and J. J. Hickman, <u>*J Lab Autom.*</u>, 2015, **20**, 107-126

431

432

433

434